1
Convergence of Experimental and Modeling Studies

Vikas Mittal

1.1
Introduction

Experimental results on composite properties are generally modeled using different finite element and micromechanical models to gain further insights into the experimental findings. Such models are also useful in predicting the properties of same or similar materials, thus eliminating the need for synthesizing each and every composite first to ascertain its properties. A number of precautions are, however, necessary to avoid discrepancies in the model outcome, for example, the model used should not have unrealistic assumptions, and the experimental results should be in plenty to have an accurate model. The following sections present some examples of modeling and prediction of polymer clay nanocomposite properties using micromechanical, finite element, and factorial design methods.

1.2
Review of Various Model Systems

A number of micromechanical models have been developed over the years to predict the mechanical behavior of particulate composites [1–4]. The Halpin–Tsai model has received special attention owing to better prediction of the properties for a variety of reinforcement geometries. The relative tensile modulus is expressed as

$$E/E_m = (1+\zeta\eta\varphi_f)/(1-\eta\varphi_f)$$

where E and E_m correspond to the elastic moduli of composite and matrix, respectively, ζ represents the shape factor, which is dependent on filler geometry and loading direction and φ_f is the inorganic volume fraction. η is given by the expression

$$\eta = (E_f/E_m - 1)/(E_f/E_m + \zeta)$$

where E_f is the modulus of the filler. The η values need to be correctly defined in order to have better prediction of the properties. For the oriented discontinuous

Modeling and Prediction of Polymer Nanocomposite Properties, First Edition. Edited by Vikas Mittal.

ribbon or lamellae, it is estimated to be twice the aspect ratio. It has been reported to overpredict the stiffness in this case; therefore, its value was reported be 2/3 times the aspect ratio [5]. Nevertheless, several assumptions prevent the theory to correctly predict the stiffness of the layered silicate nanocomposites. Assumptions like firm bonding of filler and matrix, perfect alignment of the platelets in the matrix, and uniform shape and size of the filler particles in the matrix make it very difficult to correctly predict the nanocomposites properties. Incomplete exfoliation of the nanocomposites, thus, the presence of a distribution of tactoid thicknesses, is another concern. The model has recently been modified to accommodate the effect of incomplete exfoliation and misorientation of the filler, but the effect of imperfect adhesion at the surface still needs to be incorporated [6, 7].

As a case study, tensile properties of polypropylene (PP) nanocomposites containing dioctadecyldimethylammonium-modified montmorillonite (2C18•M880) using different filler inorganic volume fraction were modeled using these micromechanical approaches [8]. The modulus of the composites linearly increased with volume fraction with an increase of 45% at 4 vol% as compared to the pure PP. As shown in Figure 1.1a, the data were fitted to the conventional Halpin–Tsai equation with $\eta = 1$, which gives a value of 10.1 for ζ, indicating that possibly in these nanocomposites it cannot be simply taken as twice the aspect ratio as generally used [9]. To account for the incomplete filler exfoliation and the presence of tactoid stacks in the composites, thickness of the particle was explained by the following equation:

$$t_{\text{particle}} = d_{001}(n-1) + t_{\text{platelet}}$$

where d_{001} is the basal plane spacing of 001 plane, n is the number of the platelets in the stack, and t_{platelet} is the thickness of one platelet in the pristine montmorillonite. Thus, in this approach, filler particles were replaced by the stacks of filler platelets [6]. Applying this treatment to the Halpin–Tsai equation, different curves have been generated based on the number of platelets present in the stack as shown in Figure 1.1b. As is evident from the figure, the experimental value of relative tensile modulus for 1 vol% OMMT composites lies near to theoretical curve with 50 platelets in the stack, but the composites with higher volume fractions of the filler could not follow the predicted rise in the modulus. The observed behavior underlines another important limitation of the theoretical models for their inability to take into account the possible decrease in *d*-spacing with increasing volume fraction. Besides, the effect of misoriented platelets on the modulus also needs to be incorporated in the model. As can be seen in the SEM micrographs in Figure 1.2, for the 3 vol% 2C18•M880 OMMT-PP nanocomposites, the filler platelets can be safely treated as random and misaligned in the matrix. Figure 1.3a shows the resulting comparison when the effects of incomplete exfoliation combined with the platelets misalignment considerations were incorporated in the Halpin–Tsai model for random 3D platelets [5]. As can be seen the number of platelets in the stack for 1 vol% composites now lie between 30 and 50 (~40). Brune and Bicerano have also refined the predictions for the behavior of nanocomposites based on the combination of incomplete exfoliation and misorientation [7]. Comparing the suggested

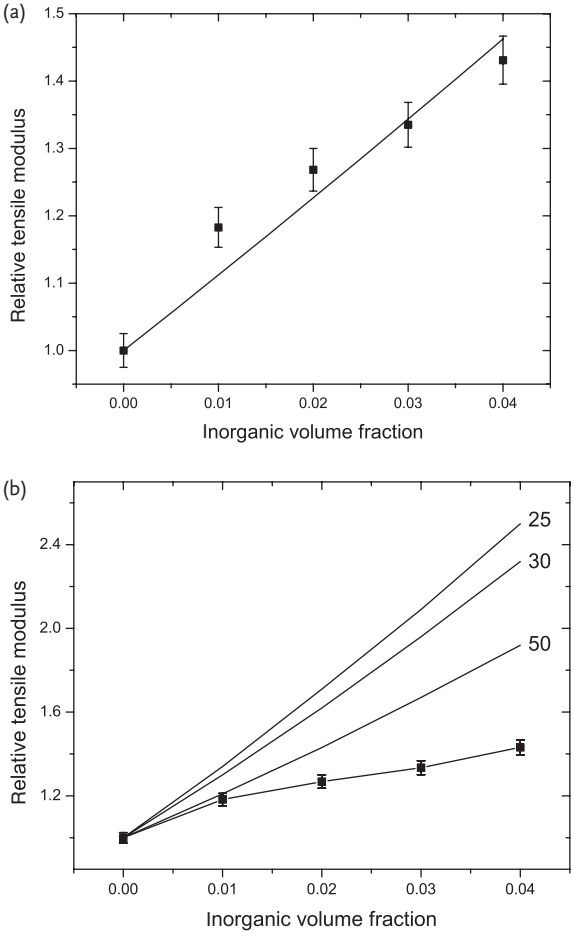

Figure 1.1 (a) Relative tensile modulus of PP nanocomposites plotted as a function of inorganic volume fraction. The solid line represents the fitting using the unmodified Halpin–Tsai equation. (b) Relative tensile modulus of the above-mentioned composites (■:- experimental) compared with the values considering different number of platelets in the stack. Reproduced from reference 8 with permission (Sage Publishers).

treatment with the experimental data, Figure 1.3b showed that the number of platelets in the stacks in 1 vol% composite was observed to be between 20 and 25, which gives an aspect ratio of about 15 for these composites. However, one major limitation of the mechanical models is the assumption of perfect adhesion at the interface, whereas the polyolefin composites studied in fact lack this adhesion, as only weak van der Waals forces can exist in the studied polymer organic monolayer systems. The theoretical results predicted above were therefore only able to match the experimental results of polar polymers due to the same reason [10, 11].

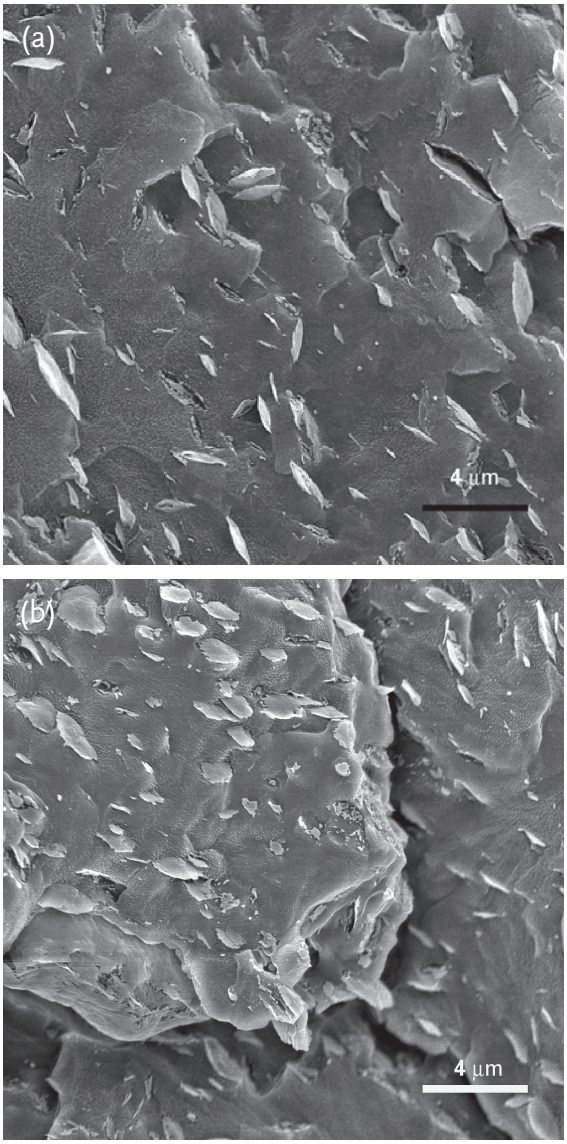

Figure 1.2 SEM micrographs of 3 vol% PP nanocomposites. Reproduced from Ref. [8] with permission (Sage Publishers).

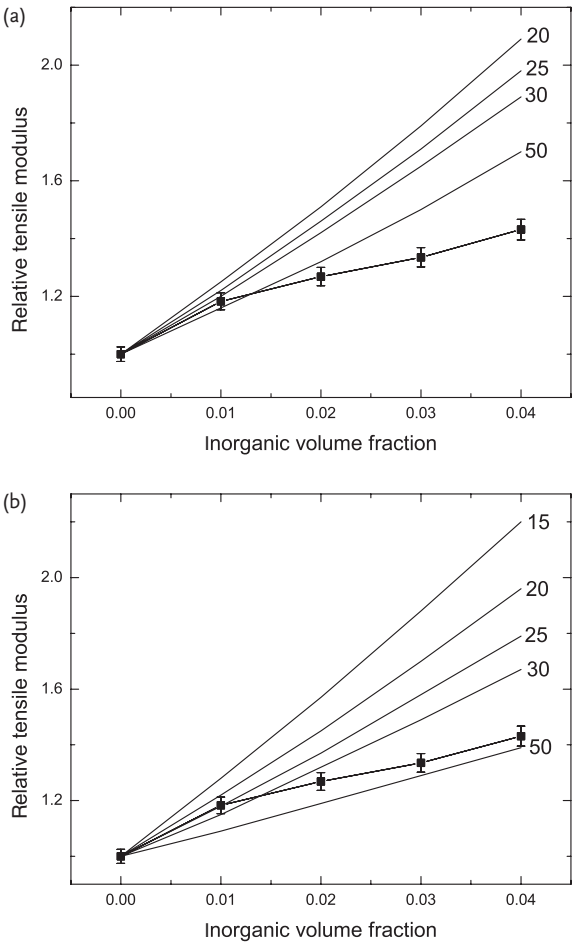

Figure 1.3 Relative tensile modulus of PP nanocomposites at different inorganic volume fraction (■:- experimental) compared with the values considering different number of platelets in the stack applying the platelet misorientation corrections. Reproduced from Ref. [8] with permission (Sage Publishers).

Nicolais and Nicodemo [12] suggested a simple model to predict the tensile strength of the filled polymers described by the equation

$$\sigma/\sigma_1 = 1 - P_1\varphi^{P2}$$

where P_1 is stress concentration-related constant with a value of 1.21 for the spherical particles having no adhesion with the matrix and P_2 is geometry-related constant with a value of 0.67 when the sample fails by random failure. The yield strength, yield strain, and stress at break for the 2C18•M880 OMMT-PP composites as a function of inorganic filler volume fraction have been plotted in Figure 1.4. The yield strength decayed with augmenting the filler volume fraction,

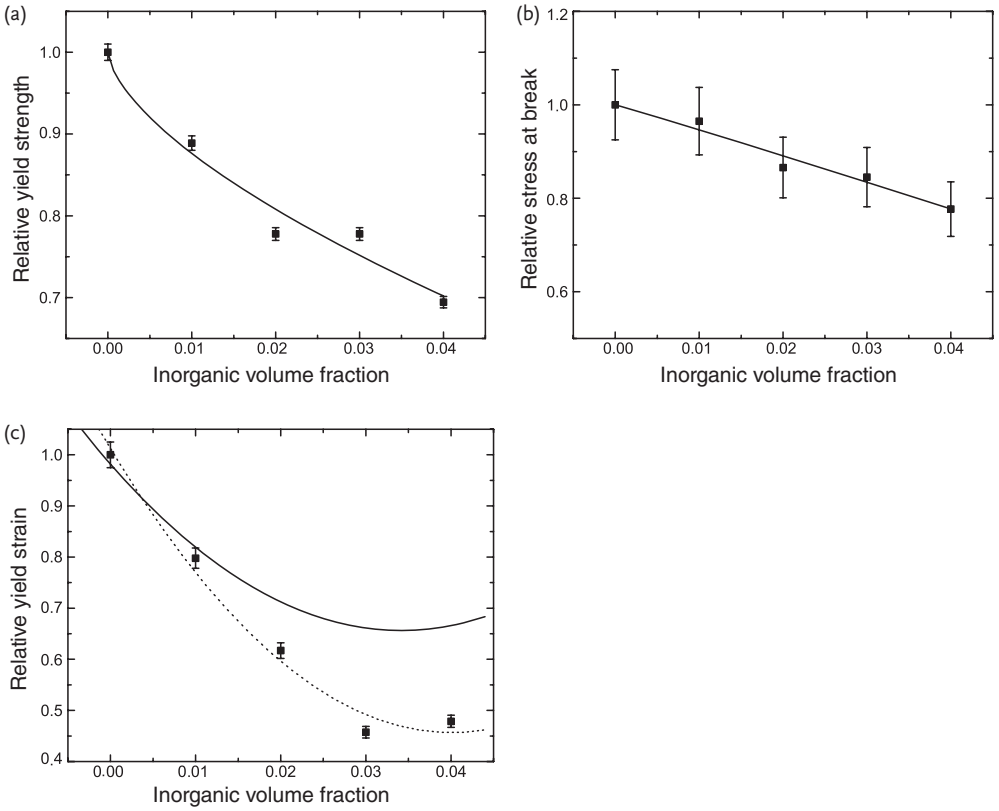

Figure 1.4 (a) Relative yield strength, (b) relative stress at break, and (c) relative yield strain of PP nanocomposites plotted as a function of inorganic volume fraction. The solid lines represent the fitting using the theoretical equations, whereas the dotted line serves simply as a guide. Reproduced from Ref. [8] with permission (Sage Publishers).

indicating the lack of adhesion at the interface and brittleness as shown in Figure 1.4a. As described earlier, with the addition of low-molecular-weight compatibilizers, an increase in the yield strengths were reported probably due to better adhesion, higher extents of delamination, and plasticization effects. The platelets in the present case, which may have been only kinetically trapped, also lead to straining of the confined polymer chains. Fitting the values of yield strength in the Nicolais and Nicodemo model yielded P_1 as 2.30 and P_2 as 0.63, thus deviating from the values marked for the spherical particles [9]. The stress at break also decreased nonlinearly with filler volume fraction owing to similar reasons and the presence of tactoids. The fitting of stress at break values (Figure 1.4b) in the model yielded P_1 and P_2 as 6.13 and 1.03, respectively, which shows higher deviation from the spherical particle predictions. Nielsen [13] suggested that the strain can be predicted by the simple equation as

$$\varepsilon_c/\varepsilon_m = 1 - \varphi_f^{1/3}$$

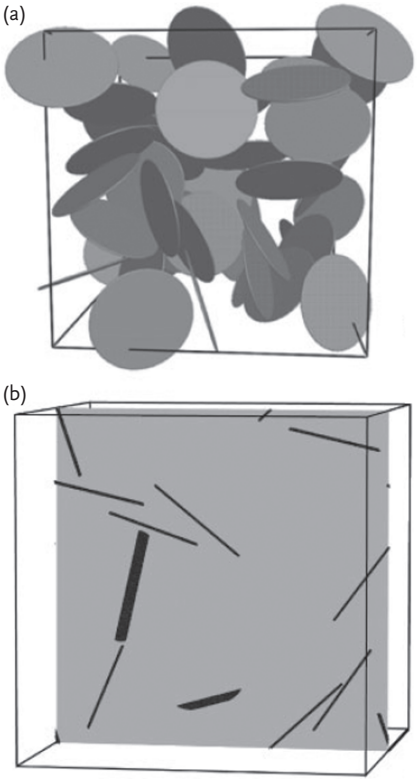

Figure 1.5 (a) A computer model comprising 50 randomly distributed and oriented round platelets with an aspect ratio of 50 at 3 vol% loading, periodic boundary conditions applied; (b) cross section through the center of the model. Reproduced from Ref. [14] with permission (Wiley).

where ε_c and ε_m are the yield strains of the composite and matrix, respectively, and φ_f is the filler volume fraction. It was assumed that the polymer breaks at the same elongation in the filled composite as the bulk unfilled polymer does. The much lower experimental values (Figure 1.4c) agree with the lack of adhesion as suggested above and the strain hardening of the confined polymer. It also indicates that the brittleness increased on increasing the filler volume fraction.

Figure 1.5a shows a typical finite element model of round platelets with an aspect ratio of 50 at 3 vol% loading, while Figure 1.5b presents a 2D-cut through the center of the model [14]. The solid lines in Figure 1.6a represent the numerical predictions for the relative permeability of composites as a function of increasing volume fraction of misaligned platelets with an aspect ratio of 50 or 100. As noted, there is excellent agreement between the experimentally measured oxygen permeability and the numerical predictions up to ca. 3 vol%. Above this concentration, it seems that the number of exfoliated layers decreases, leading to a lower average aspect ratio in both epoxy (EP) and polyurethane (PU) composites. An average

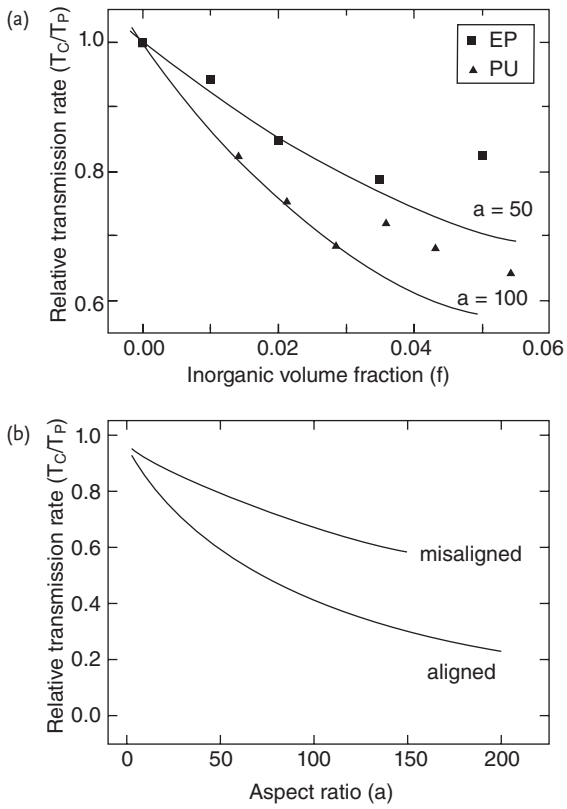

Figure 1.6 Dependence of the gas permeation through nanocomposites on the inorganic volume fraction, aspect ratio, and orientation of the platelets: (a) comparison between the measured relative oxygen permeability in EP- and PU-nanocomposites and numerical predictions; (b) influence of misalignment on the performance of platelets as permeation barrier at 3 vol% loading as predicted numerically. Reproduced from Ref. [14] with permission (Wiley).

aspect ratio of the montmorillonite platelets in nanocomposites can be estimated from the relative permeability at 3 vol% loading. The effect of misalignment on the barrier performance of platelets with different aspect ratios at 3 vol% loading, as predicted by computer models, is shown in Figure 1.6b.With increasing aspect ratio, it becomes necessary to align the platelets in order not to lose their effectiveness. Similarly, Figure 1.7 plots the comparison of measured permeability through polypropylene nanocomposites with numerical predictions for composites of parallel oriented and misaligned disk-shaped impermeable inclusions with aspect ratios (diameter/thickness) 30 and 100, respectively [15]. From this comparison, a macroscopic average of the aspect ratio for the inclusions is estimated to be between 30 and 100. However, a more precise estimation can only be made when the degree of orientation is experimentally determined and an orientation-dependent term is included in the numerical calculation.

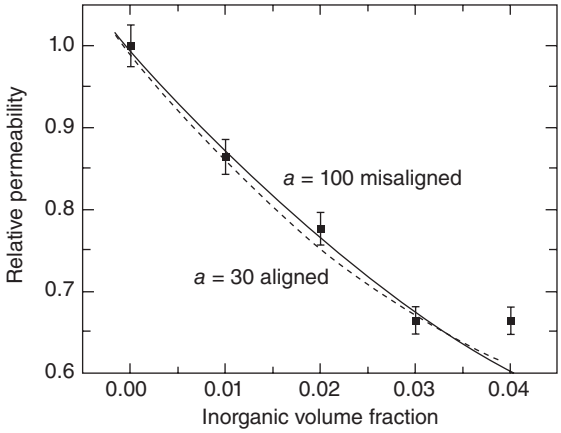

Figure 1.7 Relative permeability of the 2C18–M880-PP nanocomposites as a function of the inorganic volume fraction. The lines represent numerical predictions for composites of parallel oriented and misaligned disk-shaped impermeable inclusions with aspect ratio (diameter/thickness) of 30 and 100, respectively. Reproduced from Ref. [15] with permission (Wiley).

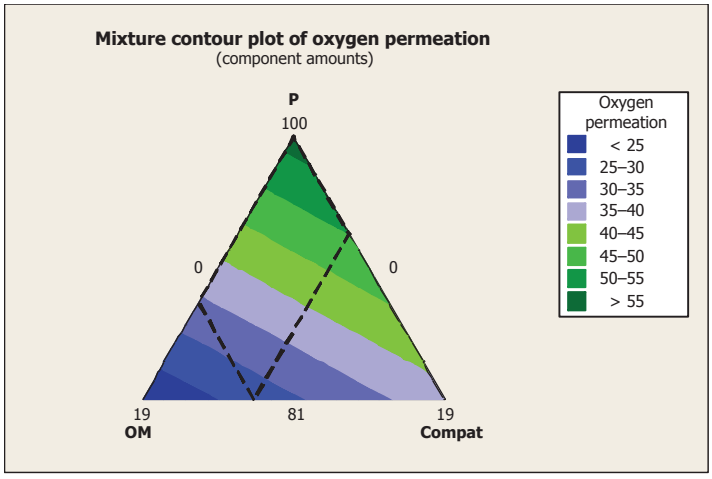

Figure 1.8 Mixture plot for the prediction of oxygen permeation of polyethylene nanocomposites with different amounts of components: polymer (P), organically modified montmorillonite (OM) and compatibilizer (Compat).

Figures 1.8 and 1.9 also demonstrate the possibility of modeling and prediction of polyethylene clay nanocomposite properties using mixture design methods. Examples of both oxygen permeation as well as tensile modulus as a function of different amounts of different components polymer, organically modified montmorillonite and compatibilizer have been shown. Like conventional models, which depend on oversimplified assumptions, these models do not suffer from these

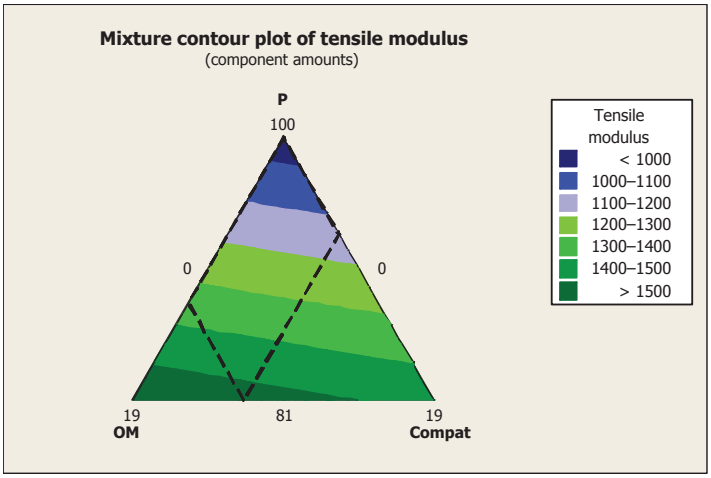

Figure 1.9 Mixture plot for the prediction of tensile modulus of polyethylene nanocomposites with different amounts of components: polymer (P), organically modified montmorillonite (OM), and compatibilizer (Compat).

limitations and can still predict the composite properties using a set of simple equations.

References

1 Kerner, E.H. (1956) *Proc. Phys. Soc.*, **B69**, 808.
2 Hashin, Z., and Shtrikman, S. (1963) *J. Mech. Phys. Solids*, **11**, 127.
3 Halpin, J.C. (1969) *J. Compos. Mater.*, **3**, 732.
4 Halpin, J.C. (1992) *Primer on Composite Materials Analysis*, Technomic, Lancaster.
5 van Es, M., Xiqiao, F., van Turnhout, J., and van der Giessen, E. (2001) *Specialty Polymer Additives: Principles and Application* (eds S. Al-Malaika, A.W. Golovoy, and C.A. Wilkie), Blackwell Science, CA Melden, MA, pp. 391–414.
6 Fornes, T.D., and Paul, D.R. (2003) *Polymer*, **44**, 4993.
7 Brune, D.A., and Bicerano, J. (2002) *Polymer*, **43**, 369.
8 Mittal, V. (2007) *J. Thermoplastic Compos. Mater.*, **20**, 575.
9 Osman, M.A., Rupp, J.E.P., and Suter, U.W. (2005) *Polymer*, **46**, 1653.
10 Luo, J.J., and Daniel, I.M. (2003) *Compos. Sci. Technol.*, **63**, 1607.
11 Wu, Y.P., Jia, Q.X., Yu, D.S., and Zhang, L.Q. (2004) *Polym. Test.*, **23**, 903.
12 Nicolais, L., and Nicodemo, L. (1973) *Polym. Eng. Sci.*, **13**, 469.
13 Nielsen, L.E. (1966) *J. Appl. Polym. Sci.*, **10**, 97.
14 Osman, M.A., Mittal, V., and Lusti, H.R. (2004) *Macromol. Rapid Commun.*, **25**, 1145.
15 Osman, M.A., Mittal, V., and Suter, U.W. (2007) *Macromol. Chem. Phys.*, **208**, 68.